Visible blind AlGaN 640×8 pixel ultraviolet focal plane arrays with low out-of-band response

Ma Ding[1,2,3], Xu Jintong[1,2], Liu Fuhao[1,2], Zhang Yan[1,2], Li Xiangyang[1,2]

(1. State Key Laboratories of Transducer Technology, Shanghai Institute of Technical Physics, Chinese Academy of Sciences, Shanghai 200083, China;
2. Key Laboratory of Infrared Imaging Materials and Detectors, Shanghai Institute of Technical Physics, Chinese Academy of Sciences, Shanghai 200083, China;
3. University of Chinese Academy of Sciences, Beijing, 100049, China)

Abstract: Out-of-band response is a very important parameter of UVFPA detectors. As a wide-gap semiconductor material, AlGaN based ultraviolet detector exhibits excellent performance of the out-of-band response and rejection in ultraviolet detection. Visible blind AlGaN 640×8 pixel ultraviolet focal plane arrays (UVFPA) detector was reported, whose spectral response range is 345-363.5 nm. To characterize the out-of-band response of the detector over a wide spectral range, by monochromatic spectral scanning, a response spectrum of the UVFPA was obtained with a wide range from UV to near IR. The result shows that the UVFPA detector has an excellent performance of out-of-band response. The ratio is 1.14% over the whole spectral band from 300 to 1 160 nm.

Key words: out-of-band response; UVFPA; visible blind

CLC number: TN23 **Document code:** A **DOI:** 10.3788/IRLA201746.S120001

具有低带外响应的 640×8 元可见盲 AlGaN 紫外焦平面

马 丁[1,2,3],许金通[1,2],刘福浩[1,2],张 燕[1,2],李向阳[1,2]

(1. 中国科学院上海技术物理研究所 传感技术国家重点实验室,上海 200083;
2. 中国科学院上海技术物理研究所 红外成像材料与器件重点实验室,上海 200083;
3. 中国科学院大学,北京 100049)

摘 要: 带外响应是紫外焦平面探测器的一个重要参数。作为一种宽禁带半导体材料,AlGaN 基紫外探测器在紫外探测领域中具有十分优秀的带外响应性能及带外抑制能力。报道了一种 640×8 元可见盲紫外焦平面探测器,其光谱响应范围为 345~363.5 nm。为了表征该焦平面探测器在宽光谱范围内的带外响应性能,使用单色仪对该器件进行了光谱扫描,扫描光谱范围涵盖了从紫外波段到近红外波段的光谱范围。其结果表示,该紫外焦平面探测器具有优秀的带外响应性能,在 300~1 160 nm 光谱范围内,光谱带外响应比率仅为 1.14%。

关键词: 带外响应; 紫外焦平面探测器; 可见盲

收稿日期: 2018-02-10; **修订日期:** 2018-05-20

基金项目: 国家自然科学基金(61106097,61204134,11304335);上海市自然科学基金(16ZR1441300)

作者简介: 马丁(1984-),男,博士生,主要从事红紫外探测器读出电路相关方向的研究。Email:mading@mail.sitp.ac.cn

导师简介: 李向阳(1969-),男,研究员,博士生导师,主要从事窄禁带半导体红外探测器和宽禁带半导体紫外探测器方面的研究。Email:lixy@mail.sitp.ac.cn

0 Introduction

As a general rule, the out-of-band (OOB) response is the spectral response in out-of-band region. The parameter of out-of-band response is defined as the ratio of the integrated response outside the 1% of peak response points of a spectral band to the integrated response of the band. In an imaging optical instrument, the OOB response may produce a radiometric bias that depends on the source of radiance being measured, and it could adversely affect product quality of imaging system. In addition, the OOB response can also affect other parameters such as dynamic range, background noise and absolute spectral response, which are parameters of great importance of imaging optical instrument and photoelectric devices [1-4]. Traditional ultraviolet detectors include photomultiplier tube, micro-channel-plate, silicon based UV enhancement devices, and so on. Since it is difficult to obtain the excellent performance of the OOB response, the research on the out of band response is mainly focused on the filter, and the out of band response of the detector is rarely reported. In fact, the traditional detectors, such as silicon detectors, have a huge response in out-of-band without filters.

With the continuous improvement of microelectronic technology, semiconductor manufacturing level and preparation process of AlGaN material, AlGaN-based UV detectors has attracted a lot of attention. Due to high quantum efficiency, visible/infrared background suppression and low dark current, AlGaN-based material has huge potential and practical applications in oil pollution, missile plume flame detection, fingerprint identification and astronomy[5-8]. Along with the change of Al composition, the energy gap changes from 3.4 eV to 6.2 eV, correspondingly, the spectral response changes from 200 nm to 365 nm, so AlGaN is an ideal material of UV detector for visible blind and solar blind device[9-10]. Furthermore, AlGaN UV detector also has excellent performance in out of band response as a direct wide gap semiconductor.

In this letter, we report a visible blind UVFPA with excellent performance in OOB response. For UVFPA, the OOB response is divided into two parts, the long wavelength response and the short wavelength response. Since the UV FPA has less sensitivity at specific wavelength, they intrinsically hold an excellent OOB response. This property gives them a strong anti-interference ability. So, the OOB response is an important figure-of-merit of UVFPA.

1 Device structure

Figure 1 shows the detector structure. Usually, the back illumination is selected in the device structure, which reduces the absorption of light in the p-GaN layers and light response in out-of-band region. Beyond that, we can also increase the OOB response by adjusting the thickness of each layer of p-i-n. As a window of the back illuminated UV FPA, n-AlGaN is usually thickened to improve the short wave OOB response. The suppression of long wave OOB response could be increased by adjusting the thickness of p-GaN layer, carrier concentration, which can change the generation and recombination of photo-generated carriers beyond 365 nm.

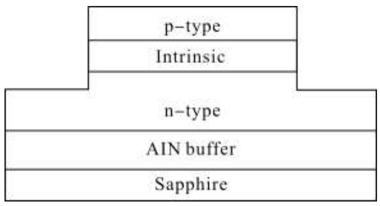

Fig.1 Schematic of a typical photodiode mesa structure

In addition, refractive index, extinction coefficient and absorption coefficient determines the ability to absorb photons. For AlGaN materials, refractive index, n is given by[11]:

$$n(\lambda)=\left[1+\frac{385}{81-E(\lambda)^2}\right]^{1/2} \quad (1)$$

where $E(\lambda)$ is incident photonsenergy. As a direct bandgap semiconductor material, absorption coefficient of AlGaN can be expressed as:

$$\alpha(\lambda)=\alpha_0\sqrt{E(\lambda)-E_g} \quad (2)$$

where E is absorbed photon energy, in experimental work, 22 $\mu m^{-1}eV^{-1/2}$ and 10.8 $\mu m^{-1}eV^{-1/2}$ have been used for value of α_0 [12]. While theoretical calculations, ignoring exitonic transitions, a value of 7.3 $\mu m^{-1}eV^{-1/2}$ has been used[11]. Here, α_0= 10 $\mu m^{-1}eV^{-1/2}$ is used. The variation of α with mole fraction x in the ternary $Al_xGa_{1-x}N$ system is assumed to occur only via the change in bandgap, which can be expressed as:

$$E_g(Al_xGa_{1-x}N)=xE_g(AlN)+(1-x)E_g(GaN)-bx(1-x) \quad (3)$$

The bowing parameter b is 1 eV [13], and then the Al fraction is calculated to be 0.098.

The extinction coefficient k is calculated from the relation[14]:

$$k=\frac{\alpha\lambda}{4\pi} \quad (4)$$

According to the above theory, we can determine the structure and the material parameters of the device, as shown in Fig.2.

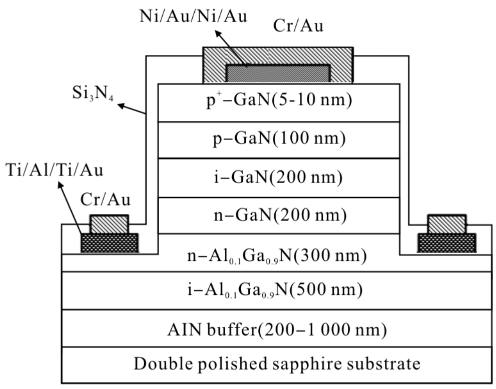

Fig.2 Schematic cross section of the epitaxial layer structure for the GaN p-i-n photodiodes of the visible blind photodetector

The films were grown on the substrate by Metal-Organic Chemical Vapor Deposition (MOCVD) on a double throw sapphire substrate. In order to reduce the dislocation and stress between AlGaN film and substrate, AlN buffer layer must be deposited on the substrate at low temperature. Then, intrinsic $Al_{0.1}Ga_{0.9}N$ films, Mg doped p type $Al_{0.1}Ga_{0.9}N$, n-GaN and i-GaN films were sequentially grown. Finally the p-GaN films were deposited on the top of the sample. After the growth of the material, the device is fabricated by photolithography, corrosion, annealing, passivation, and electrode evaporation. n-electrode and P-electrode generally use Cr/Au materials with good ohmic contact, which are connected with n type $Al_{0.1}Ga_{0.9}N$ film and p^+-GaN film.

2 Readout circuit and parameters of the UVFPA

As a hybrid focal plane array, apart from the detector, we also need to combine the readout circuit (ROIC) performance, test instrument performance and test results, so as to understand OOB mechanism more thoroughly.

Figure 3 shows the analog signal chain for the ROIC. The ROIC is designed to work in snapshot mode, all pixels are reset simultaneously. The input stage adopts the capacitive feedback trans-resistance amplifier (CTIA) structure, and the value of integrating capacitor is 62.5 fF in this stage. The following module is sampling circuit which can effectively reduce the FPN noise by using correlated double sampling (CDS) techniques. Then sampling signal transfers through the column buffer and outputs to the outside of the chip.

Figure 4 shows the fabricated visible blind 640×8 pixel UVFPA, which connected the AlGaN detector array and the ROIC through indium bumps. The center to center distance of pixel is 25 μm.

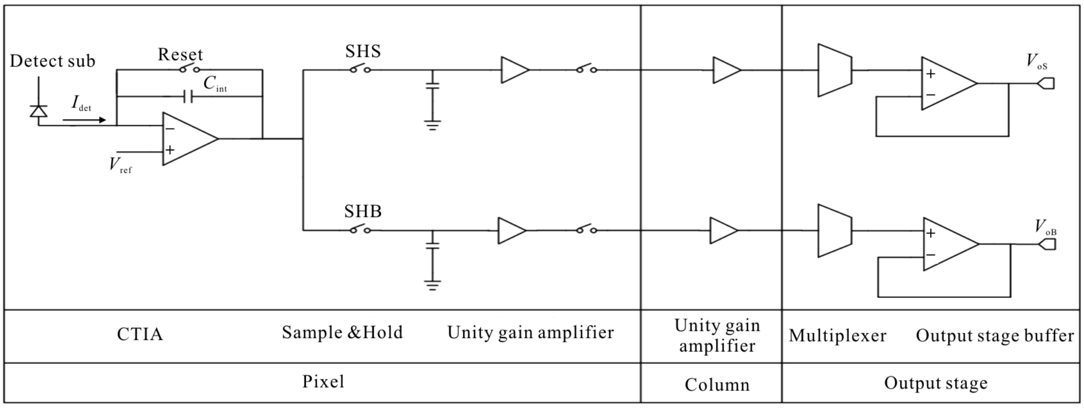

Fig.3 Analog signal chain for the readout circuit

Fig.4 Microphotograph of the fabricated visible blind 640×8 pixel UVFPA

The measurements of the UVFPA were performed with a 450 W Xe arc lamp, an iHR 550 monochromator, an integration sphere and a data acquisition and processing system in a synchronous detection scheme. The sample was uniformly illuminated from the front side. Figure 5 shows the structure of the test system. And the main characteristics of the UVFPA were summarized in Tab.1. From Tab.1 we can see that the UVFPA has excellent performance, especially the low noise, which allows the UVFPA to show a lower response in out-of-band region.

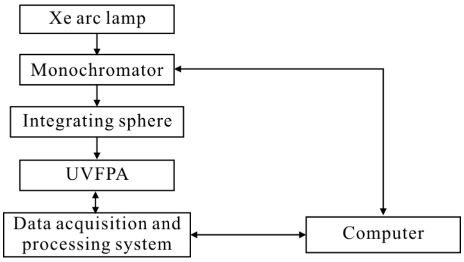

Fig.5 Structure of the test system for the measurements of the UVFPA

Tab.1 Summary data of the visible blind 640×8 pixel UVFPA

Item	Parameter
Array format/pixel	640×8
Pixel size/μm×μm	25×25
Fill factor	0.77
Unoperable pixel rate	0.28%
Pixel sensitivity/μV/e-	2.6
Output range/V	3.5
Noise/mV	0.25
Linear dynamic range/dB	81
Pixel data rate/kHz	200
Responsivity non-uniformity	4.7%
Linearity	99.3%
Frame rate/Hz	20
Power supply/V	5
Power consumption/mW	150

Furthermore, we carried out push-broom imaging by using the fabricated visible blind 640×8 pixel UVFPA. The image taken with the UVFPA is shown in Fig.6. Benefit from good

Fig.6 UV image taken with the fabricated visible blind 640×8 pixel UVFPA

performance of the UVFPA, we can clearly see that the image quality is excellent.

3 Spectral response and discussion

In order to fully reflect the out-of-band spectral response of the UVFPA, the spectral response is measured in this test, spectrum range is from 300 nm to 1 100 nm and the spectrum resolution is 1 nm. In addition, to obtain the absolute spectral response, a calibrated Si detector and a C9329 preamplifier was used for calibrating spectral energy of the Xe arc lamp. In this test, the calibrated Si detector is S1336 fabricated by Hamamatsu, and the spectral response range of the calibration data is 200-1 160 nm. The pixel responsivity of the UVFPA is calculated according to Eq.(5):

$$R(i,j)=\frac{V_s(i,j)A_{0s}R_{0s}}{\alpha V_{0s}A_D} \tag{5}$$

where $R(i,j)$ is the responsivity of the pixel which is row i and column j in FPA at the wavelength of λ. A_{0s} is the effective photosensitive area of the calibrated Si detector. R_{0s} is the responsivity at the wavelength of λ of the calibrated Si detector, α is the coefficient of uniformity correction of the light spot, the value of this parameter is 1 in this measurement because of using integrating sphere. V_{0s} is the response voltage of the calibrated Si detector. A_D is the pixel area of the focal plane array which is tested.

The responsivity of the UVFPA is then obtained by:

$$\overline{R}=\frac{1}{(M\times N-D)}\left[\sum_{i=1}^{M}\sum_{j=1}^{N}R(i,j)-\sum_{(i,j)\in D}R(i,j)\right] \tag{6}$$

where $\overline{R}$ is the responsivity of the UVFPA. M and N is the number of columns and rows of the UVFPA. D is the number of unoperable pixels, which include dead pixels and overheating pixels. And the normalized spectral response curve shows in Fig.7.

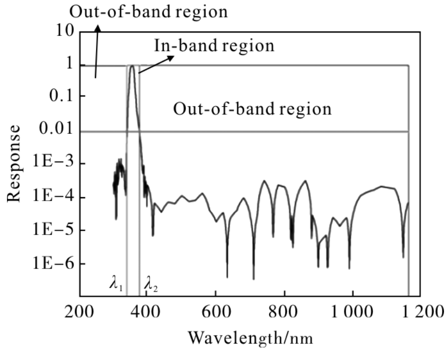

Fig.7 Normalized spectral response of the visible blind UVFPA

From the curve shown in Fig.6, we can get the wavelength λ_1 and λ_2 which are corresponding 1% of the peak value. In this calculation, the solar spectrum is used as incident condition, so the OOB response ratio is calculated from the following relation:

$$R_{OOB}=\frac{\int_{300}^{\lambda_1}S(\lambda)R(\lambda)d\lambda+\int_{\lambda_2}^{1\,160}S(\lambda)R(\lambda)d\lambda}{\int_{\lambda_1}^{\lambda_2}S(\lambda)R(\lambda)d\lambda} \tag{7}$$

where R_{OOB} is the OOB response ratio, $R(\lambda)$ is relative spectral response of the UVFPA, $S(\lambda)$ is standard solar spectrum. By using Eq.(6), the value of OOB response ratio of this UVFPA is 1.14%. And through the above spectrum measurement results, we obtained otherparameters associated with the spectrum of the UVFPA as listed in Tab.2.

Tab.2 Parameters associated with the spectrum of the UVFPA

Item	Parameter
Cuton wavelength/nm	345
Cutoff wavelength/nm	363.5
Δλ/nm	18.5
Peak quantum efficiency	51.2%
OOB response	1.14%

4 Conclusion

In this paper, we made a brief analysis of the factors related to the OOB response in device structure and materials performance. And then, through the analysis result, we determined the device structure and corresponding parameters. In addition, we also introduced the readout circuit and fabricated a AlGaN-based visible blind 640×8 pixel UVFPA, which has good performance and excellent imaging quality. In order to represent the OOB response of the UVFPA, spectral characterization was performed over the range of 300 nm to 1 160 nm. Spectral response range of the UVFPA is 345-363.5 nm. The spectral response curve also indicated the UVFPA has very low out-of-band response, and the value of OOB response ratio of this UVFPA is 1.14%.

References:

[1] Chen W. Optimal out-of-band correction for multispectral remote sensing [J]. ***IEEE Transactions on Geoscience & Remote Sensing***, 2012, 51(33): 7962-7968.

[2] Gao B C, Chen W. Multispectral decomposition for the removal of out-of-band effects of visible/infrared imaging radiometer suite visible and near-infrared bands [J]. ***Applied Optics***, 2012, 51(18): 4078-4086.

[3] Gordon H R. Remote sensing of ocean color: a methodology for dealing with broad spectral bands and significant out-of-band response[J]. ***Applied Optics***, 1995, 34(36): 8363-8374.

[4] Kelcey J, Lucieer A. Sensor correction of a 6-band multispectral imaging sensor for UAV remote sensing [J]. ***Remote Sensing***, 2012, 4(5): 1462-1493.

[5] Zhang Y, Chu K, Shao X. GaN-based 512×1 ultroviolet linear focal plane arrays [J]. ***Acta Optica Sinica***, 2009, 29 (12): 3515-3518.

[6] Rogalski A, Razeghi M. Semiconductor ultraviolet photodetectors [J]. ***Opto-Electronics Review***, 1996, 4(13): 13-30.

[7] Brosch N. Exotic UV astronomy [J]. ***Astrophysics & Space Science***, 2009, 320(1-3): 207-215.

[8] Monroy E, Hamilton M, Walker D. High-quality visible-blind AlGaN p-i-n photodiodes [J]. ***Applied Physics Letter***, 1999, 74 (8): 1171-1173.

[9] Shur M S, Gaska R, Bykhovski A. GaN-based electronic devices[J]. ***Solid-State Electronics***, 1999, 43(8): 1451-1458.

[10] Walker D, Saxler A, Kung P. Visible blind GaN pin photodiodes [J]. ***Applied Physics Letters***, 1998, 72(25): 3303-3305.

[11] Wang R, Ruden P P, Kolink J. Dielectric properties of wurtzite and zincblende structure gallium nitride [J]. ***Journal of Physics and Chemistry of Solids***, 1997, 58(6):913-918.

[12] Zhang X, Kung P, Walker D. Photovoltaic effects in GaN structures with p-n junctions [J]. ***Applied Physics Letters***, 1995, 67(14): 2028-2030.

[13] Yun F, Reshchikov M A, He L. Energy band bowing parameter in $Al_xGa_{1-x}N$ alloys [J]. ***Journal of Applied Physics***, 2002, 92(8): 4837-4839.

[14] Li C, Bao X, Xu J. Optical characterization of GaN/AlGaN bilayer by transmission and reflection spectra [J]. ***Journal of Applied Physics***, 2013, 108(6): 063104.